Holographic Characterization of the Onsala Twin Telescopes

Mugundhan V., Handirk R., Hovey G., Lerner M.S., Le Bail K., Haas R.

Abstract Holography is a technique that uses the complex electric field distribution to calculate the aperture amplitude and phase distribution of the Antenna Under Test (AUT). They can be used to infer the aperture efficiency, ray path length, and surface error distributions. We applied this technique to the Onsala Twin Telescope, where we used a geostationary satellite at a low elevation as the source. We used a real-time cross-correlator to obtain the visibilities, which were then inverted to estimate the aperture efficiency and ray-path lengths of both the Onsala Twin Telescopes (OTT). We find that the telescopes have an efficiency of $\sim 43\%$ and 40 %, and a rms ray path length $\sim \leq$ 1.5 mm. The decoupling of the effect of primary, secondary, and feed is currently underway. Further measurements at different elevations will be presented in the future.

Keywords Holography, Correlator, Aperture efficiency, Ray path length

1 Introduction

The VLBI2010 Global Observing System (VGOS) aims to achieve improved position accuracy compared to legacy systems, generating Earth orientation parameters and station position products with a cadence of less than one day (Petrachenko et al., 2009). It seeks to achieve this through an increase in the number of observations and minimizing systematics. Achieving these ambitious goals requires dishes that are able to slew fast, wide-band feeds, and low-noise receiver systems, data recording over a large bandwidth, and near real-time correlation.

In line with these requirements, two new dishes —the Onsala Twin Telescopes (OTT) —of 13.2 m diameter, with fast slew rates, were commissioned at the Onsala Space Observatory(Elgered et al., 2017). To maximize the aperture efficiency, these dishes use ring focus Gregorian optics (Venter et al. (2023), refer to figure 1). The dishes use a Quad ridged feed horn on the ONSA13NE, and an Eleven feed on the ONSA13SW, with the former operating from 3 GHz —14 GHz, while the latter covers a bandwidth of 2 GHz —14 GHz. These telescopes, since their inception, have regularly participated in both legacy and VGOS sessions, and have also been used for other science goals as a standalone, two-element interferometer (Varenius et al., 2022).

In addition to this, the OTT have also been used to monitor the unintended emission from large satellite constellations in the low earth orbit (LEO) on protected bands within 10 —13 GHz (Hovey et al., 2025). This is important to inform on the interference mitigation strategy for both VGOS and upcoming large astronomical observatories like the Square Kilometer Array (SKA).

To ensure that the required performance is achieved and maintained by the OTT, it becomes important to monitor different parameters like Aperture efficiency (η), System temperature (T_{sys} regularly, as they affect the minimum detectable flux as:

Mugundhan V. [1,2]
(1) Department of SPASE, IIT Kanpur, Kanpur 208016, India,
(2) Onsala Space Observatory, Department of Space, Earth and Environment, Observatorievägen 90, 439 94 Sweden
Handirk R., Lerner M.S., Le Bail K., Haas R. [1]
(1) Onsala Space Observatory, Department of Space, Earth and Environment, Observatorievägen 90, 439 94 Sweden
Hovey G. [3]
(3) CygnusTech Pvt. Ltd., Canada

$$\Delta S_{min} = \frac{2kT_{sys}}{\eta A_p \sqrt{\beta\tau}} \quad (1)$$

where k is the Boltzmann constant, A_p is the area of the physical aperture, and β and τ are the integration bandwidth and time.

β and τ are user programmable; regular measurements of T_{sys} can be made using a noise switching system during observations. η is a product of various sub-efficiencies such as ground noise pick-up, feed-efficiency, reflector surface accuracy, etc. This can be characterized using simulations of the dish optics using dedicated software, viz. GRASP, and the surface accuracy of the reflector can be measured using techniques such as photogrammetry. However, to fully characterize the path of the electromagnetic wave, a more holistic approach is required, which is provided by *holography*.

2 Method

Holography is based on the Fourier relation between the aperture and field domains (Perley, 2021). The far-field distribution, E_{ff} of an aperture can be written as:

$$E_{ff}(l,m) = \int_{-\inf}^{+\inf}\int_{-\inf}^{+\inf} A(u,v)e^{-j2\pi(ul+vm)}dudv \quad (2)$$

where A is the aperture distribution, which is a function of $u = \frac{x}{\lambda}$ and $v = \frac{y}{\lambda}$, while l,m are direction cosines. This relation is valid for small pointing offsets from the bore-sight, which is indeed the case here.

The antenna under test (AUT) and the reference antenna, the former scanning across and the latter tracking a strong source, form the interferometer, which is used to effectively measure the E_{ff}. Once this has been measured, the relation described in Equation 2 can be used to invert E_{ff} to obtain $A(u,v)$.

In our case, both antennas were used as reference and AUT during different parts of the campaign. We used a geostationary satellite as the reference source, as it provides a strong signal and allows the reference antenna to be almost stationary. To measure the performance of the dish over different elevations, we plan to use celestial sources too, but these results will be presented elsewhere.

The radio frequency (RF) signals from both the OTTs are transmitted to the receiver room through optical fibers $\approx$ 1 km long. They are converted back to electrical signals using the fiber to RF receiver, and power split just after the RF monitoring system, and fed to an independent receiver system.

The receiver system used a mixer to down-convert the RF signal from the antenna to an IF in the range of 30 MHz to 1 GHz. A QuickSYN[1] RF synthesizer, synchronized to the 10 MHz maser source, was used to generate the local oscillator (LO) signal. The synthesizer was controlled using a Revolution Pi[2], where a python script was developed to set the LO frequency and power.

The cross-correlation between the AUT and the reference can be used to map the far-field electric field distribution. For this purpose, we implemented a wideband FX correlator firmware on an RFSoC 4x2 evaluation board[3]. This board takes 4 analog inputs, enabling us to obtain full polarization measurements. As the board has an AMD Zynq MPSoC[4], which has both Programmable logic and Processor system, the correlation logic is implemented on the former, while the Ethernet data transmission is implemented in the latter. As we have 4 inputs, we compute 4 auto-correlations (AC) and 6 cross-correlation (CC) products. Each AC and CC has 1024 channels with 1 MHz resolution and is integrated in time for 1s. They are then packetized and published using the ZeroMQ framework[5]. The data acquisition system that captures these packets "subscribes" to them and forwards them to a routine to plot the correlations to a webpage, and another to save the data to an HDF5 file.

3 Scan Strategy and Data Analysis

We used the daily two-line element sets published by NORAD for EUTELSAT 16A (175.177°, 24.626°) to gener-

[1] https://www.keysight.com/blogs/en/tech/rfmw/2023/10/23/drop-in-replacement-for-quicksyn-fsw-0020

[2] https://revolutionpi.com/de

[3] https://www.amd.com/en/corporate/university-program/aup-boards/rfsoc4x2.html

[4] https://www.amd.com/en/products/adaptive-socs-and-fpgas/soc/zynq-ultrascale-plus-rfsoc.html#product-table

[5] https://zeromq.org/

ate accurate pointing and tracking information for the holographic measurements. To obtain fine information on aperture illumination, a wide scan is required. However, this results very long holography runs. To strike a balance between the two, we carried out measurements with a scan extent of $\approx 38\frac{\lambda}{D}$, where λ is the wavelength of observation, and D is the dish diameter. This resulted in an aperture spatial resolution of $\approx$ 345 mm. The angular spacing, $\Delta\theta$, between each step in a scan was $\approx \frac{\lambda}{2kD}$, where k is the oversampling factor. Using k=1.4 gave us an $\Delta\theta$ of $\approx$ 0.04°. A schematic of the scan strategy is shown in Figure 1

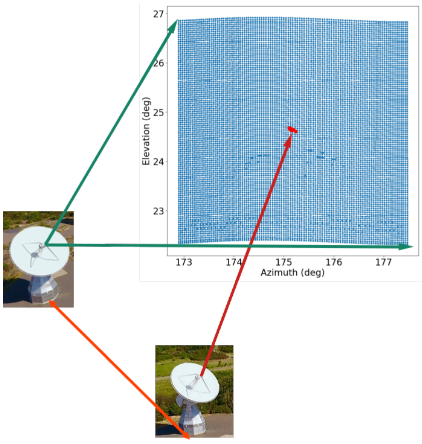

Fig. 1 The plot shows the scan strategy, where the antenna at the bottom-right tracks the reference, while the one at center left scans across a 4.9°across it. The blue dots are the scan-grid points, spaced at 0.042°.

The data analysis routine was developed in Python[6]. The hdf5[7] file is read and any missing data is filled based with NaN values, to maintain continuity in time. The observation logs from BIFROST (Lerner, 2022), the telescope control and monitoring software interface at OSO, were used to separate the reference pointings from the scans. The reference pointings were then used to calibrate the time- and frequency-dependent complex gains.

The calibrated data were then gridded in azimuth (az) and elevation (el). There power and phase distribution are verified visually to ensure that they resemble expected patterns (refer Figure 2). After this, the data is inverted to obtain the distribution in the Aperture plane (refer Figure 3).

[6] `https://www.python.org/`

[7] `https://www.hdfgroup.org/solutions/hdf5/`

4 Interpretation and Results

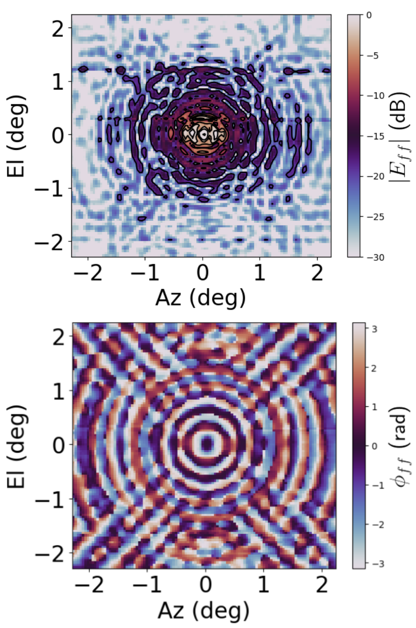

Fig. 2 The far-field electric field amplitude (top) and phase (bottom) measured in the X Polarization of ONSA13NE.

Figure 2 shows the far-field amplitude (top panel) and phase (bottom panel) of the X-polarization from the ONSA13NE. The main lobe's maximum is at $\approx$ 0 °. We also note that there are a lot of high frequency structures seen in the beam. The diagonal structures can be attributed to the feed-legs. In the phase plot, close to the boresight, the phase is zero, and starts to fluctuate between $\pm\,\pi$ across the field of view, which is again consistent with geometric delay increasing as we go away from the phase center. Similar structure was observed when ONSA13SE was the AUT as well.

We used the far-field patterns of the ONSA13NE's X-Pol simulated using GRASP[8] to obtain the simulated aperture efficiency. For the dish using the quad ridge feed horn (QRFH), we estimated an $\eta \approx 57\%$ (Flygare

[8] `https://www.ticra.com/software/grasp/`

et al., 2017). We then used this as a reference to compare it with our measurements (see Figure 3.

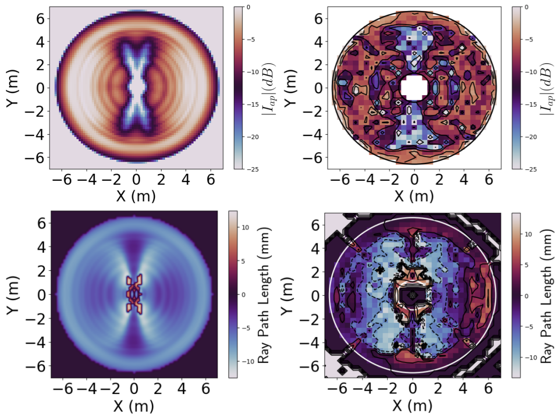

Fig. 3 The simulated (left) and the measured (right) aperture illumination (top) and ray path length (bottom).

In both the simulations and in the measurements of the aperture illumination, we see a "bunny ear" which has been attributed to some inaccuracy during the assembly of the QRFH. We also observe the blockage in the aperture provided by the feed-legs. The small and the large black circles represent the size of the secondary and the primary reflectors respectively. By integrating along the available aperture, the same technique we used when analyzing the simulated data, we found an $\eta \approx 43$ % across both polarizations. Performing a similar analysis on the ONSA13SW, we found an $\eta \approx 40$ % across both polarizations.

We converted the aperture plane phases to ray path length. In the phase plot too, we see large deviations close to and within the boundary of the "bunny-ears", however outside this region, the phase is pretty uniform. An rms ray path length deviation of $\approx$ 1.5 mm is found. This is consistent with the results from Lösler et al. (2019), which considers only the primary surface.

5 Conclusions and outlook

We have presented results from holography measurements of the OTTs using a geostationary satellite as the reference source. Using these measurements, we estimate the aperture efficiency of both ONSA13NE and ONSA13SW to be $\approx 43\%$ and 40%, respectively. We also found an rms ray path length of $\approx$ 1.5 mm for both dishes, which is consistent with photogrammetric measurements of the primary reflectors. In the future, we will perform extensive simulations using a model for the Eleven feed as well. We will also further decouple the different sub-efficiencies and path length contributions to account for the measured values. We plan on performing holography measurements on celestial sources like Cyg-A, Cas-A etc., so the beam and aperture can be studied over the entire frequency band and polarizations.

References

Flygare J, Pantaleev M, Billade B, Dahlgren M, Helldner L, Haas R (2017) Sensitivity and antenna noise temperature analysis of the feed system for the Onsala twin telescopes. *Proc. 23rd EVGA Working Meeting (EVGA2017), Gothenburg, Sweden.*

Perley R (2021) VLA Holography. *EVLA Memo 212*, National Radio Astronomy Observatory.

Petrachenko B, Niell A, Behrend D, Corey B, Böhm J, Chralot P, Collioud A, Gipson J, Haas R, Hobiger T, et al. (2009) Design aspects of the VLBI2010 systemfffiProgress report of the IVS VLBI2010 committee. *Technical Report*, IVS VLBI2010 Committee.

Elgered G, Haas R, Conway J, Hammargren R, Helldner L, Hobiger T, Pantaleev M, Wennerbäck L (2017) The Onsala twin telescopes project. *Proc. 23rd EVGA Working Meeting (EVGA2017), Gothenburg, Sweden.*

Lösler M, Haas R, Eschelbach C, Greiwe A (2019) Gravitational deformation of ring-focus antennas for VGOS: first investigations at the Onsala twin telescopes project. *Journal of Geodesy*, 93(10), 2069–2087.

Venter M, Garcia-Pérez Ó, Tercero-Martínez F, López-Pérez JA, Malan S, Mey P (2023) Performance of the VGOS Radio Telescope with As-built Feed and Geometry Using Electromagnetic Simulations. *Proc. 17th European Conference on Antennas and Propagation (EuCAP)*, 1–4, IEEE.

Varenius E, Maio F, Le Bail K, Haas R (2022) Broad band flux-density monitoring of radio sources with the Onsala twin telescopes. *Experimental Astronomy*, 54(1), 137–155.

Hovey G, Vijayaraghavan M, Di Vruno F, Haas R, Le Bail K, Chin Chuan L (2025) LEO Satellites and Antenna Performance Investigations with the Onsala Twin Telescopes. *Proc. International VLBI Service for Geodesy and Astrometry 2024 General Meeting*, p. 11.

Lerner M (2022) *The BIFROST Userffftts Handbook*. BIFROST Collaboration.